DESY 22-037, TUM-HEP-1389-22

Revealing the Cosmic History with Gravitational Waves

Andreas Ringwald[1]* and Carlos Tamarit[2]†
[1] *Deutsches Elektronen-Synchrotron DESY, Notkestr. 85, 22607 Hamburg, Germany and*
[2] *Physik-Department T70, Technische Universität München, James-Franck-Straße, 85748 Garching, Germany*

The characteristics of the cosmic microwave background provide circumstantial evidence that the hot radiation-dominated epoch in the early universe was preceded by a period of inflationary expansion. Here, we show how a measurement of the stochastic gravitational wave background can reveal the cosmic history and the physical conditions during inflation, subsequent pre- and reheating, and the beginning of the hot big bang era. This is exemplified with a particularly well-motivated and predictive minimal extension of the Standard Model which is known to provide a complete model for particle physics –up to the Planck scale– and for cosmology –back to inflation.

Introduction.—Big Bang cosmology describes how the universe expanded from an initial state of extremely high density into the cosmos we currently inhabit. It comprehensively explains a broad range of observed phenomena, including the abundance of light elements, the Cosmic Microwave Background (CMB) radiation, and the large-scale structure. It successfully delineates the cosmic history back to at least a fraction of a second after its birth, when the primordial plasma was radiation-dominated and Big Bang Nucleosynthesis (BBN) took place, at temperatures around a few MeV.

Direct information about the cosmic history prior to BBN may be obtained from the observation of Gravitational Waves (GWs). In fact, after their production they freely traverse cosmic distances, making them a unique probe of the very early universe [1, 2]. An eventual measurement of the complete spectrum of primordial stochastic GWs may inform us in particular about three cosmological events supposed to occur in cosmic history: *i)* a stage of inflationary expansion preceding the radiation-dominated era, *ii)* the subsequent pre- and reheating stages, and *iii)* the beginning of the hot thermal radiation-dominated era after reheating.

The corresponding GW predictions are model-dependent. They depend crucially on the field content and its dynamics, in particular on the parameters determining the scale of inflation and the reheating temperature. To get the complete picture, one needs a complete model for particle physics and cosmology, such as for example the Standard Model*Axion*Seesaw*Higgs portal inflation (SMASH) model [3–5] – a well motivated and predictive minimal extension of the Standard Model of particle physics (SM) which addresses five fundamental problems of particle physics and cosmology in one stroke: inflation, baryon asymmetry, neutrino masses, strong CP problem, and dark matter.

In two preceding publications we have determined the GW spectra in SMASH originating from quantum fluctuations during inflation [6] and from thermal fluctuations at the beginning of the hot thermal radiation-dominated stage [7]. In this Letter we determine the GW spectrum arising from inflaton fragmentation during preheating [8–15] and provide improved estimates of the reheating temperature and the ensuing spectrum of GWs from the thermal plasma. To the best of our knowledge, this represents the first computation of the complete spectrum of stochastic GWs generated in the early universe for a particular particle physics model [16], cf. Fig. 1.

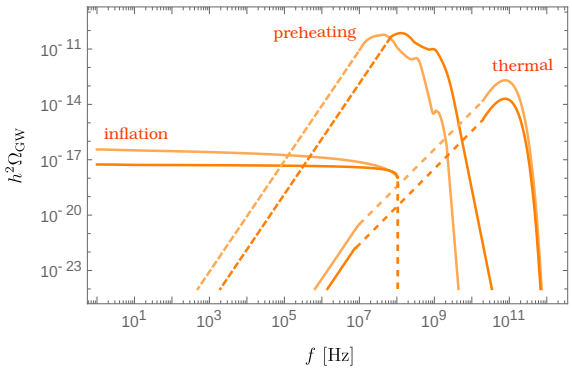

FIG. 1. Today's fractional contribution of primordial GWs to the energy density in the universe per logarithmic frequency interval, $h^2\Omega_{\rm GW}$, versus the frequency, f, as predicted in SMASH for the benchmark points 1 (lighter) and 2 (darker).

The SMASH model.—In the SMASH model [3–5], a new complex scalar field σ (the Peccei-Quinn (PQ) field), a vector-like quark Q and three singlet neutrinos N_i, with $i = 1, 2, 3$, are added to the SM. All the new fields, as well as the quarks and leptons of the SM, are assumed to be charged under a global $U(1)_{\rm PQ}$ symmetry. The scalar potential in SMASH, which involves also the Higgs doublet H (neutral under PQ), has the general form:

$$\begin{aligned} V(H,\sigma) =& \lambda_H \left(H^\dagger H - \frac{v^2}{2}\right)^2 + \lambda_\sigma \left(|\sigma|^2 - \frac{v_\sigma^2}{2}\right)^2 \\ &+ 2\lambda_{H\sigma} \left(H^\dagger H - \frac{v^2}{2}\right)\left(|\sigma|^2 - \frac{v_\sigma^2}{2}\right) . \end{aligned} \tag{1}$$

Here, the dimensionless couplings are assumed to obey $\lambda_H, \lambda_\sigma > 0$, $\lambda_{H\sigma}^2 < \lambda_H \lambda_\sigma$, in order to ensure that the PQ and electroweak symmetries are broken by the vacuum expectation values $\langle H^\dagger H \rangle = v^2/2$, $\langle |\sigma|^2 \rangle = v_\sigma^2/2$, where $v_\sigma \gg v = 246\,\mathrm{GeV}$. The hypercharge of the vector quark Q and the PQ charges of the SM fermions are chosen such that the only allowed interactions of the exotic fermions N_i, Q are $\mathcal{L} \supset -[F_{ij} \bar{N}_j P_L L_i \epsilon H + \frac{1}{2} Y_{ij} \sigma \bar{N}_i P_L N_j + y\, \sigma \bar{Q} P_L Q + y_{Q_{di}} \sigma \bar{D}_i P_L Q + h.c.]$. In the previous formula the fermion fields are four-component spinors. D_i, L_i denote the Dirac spinors associated with the down quarks and leptons of the ith generation, while the N_i are taken to be Majorana spinors. In this model the strong CP problem is solved by the PQ mechanism [17]. The axion [18, 19] – the pseudo Goldstone boson associated with the spontaneous breaking of the PQ symmetry – can be the main constituent of dark matter if its decay constant $f_a = v_\sigma \sim 10^{11}\,\mathrm{GeV}$ [20–22]. The PQ symmetry breaking scale also gives rise to large Majorana masses for the heavy neutrinos. This can explain the smallness of the active neutrinos' masses through the seesaw mechanism [23–26] and also results in the generation of the baryon asymmetry of the universe via thermal leptogenesis [27].

The cosmic history in SMASH.—Inflation results from the dynamics of the PQ and Higgs fields in the presence of non-minimal couplings to the Ricci scalar R [28–32],

$$S \supset -\int d^4x\sqrt{-g}\left[\frac{M^2}{2} + \xi_H\, H^\dagger H + \xi_\sigma\, \sigma^*\sigma\right] R\,. \quad (2)$$

Here, the mass scale M is related to the reduced Planck mass ($M_P \simeq 2.435 \times 10^{18}\,\mathrm{GeV}$) by $M_P^2 = M^2 + \xi_H v^2 + \xi_\sigma v_\sigma^2$. After a Weyl transformation of the metric to the Einstein frame, which eliminates the non-minimal gravitational couplings, the potential becomes flat for large field values. Problems with perturbative unitarity [33, 34] are avoided by requiring $1 \gtrsim \xi_\sigma \gg \xi_H \geq 0$; we will neglect ξ_H in the following. To ensure a viable reheating scenario, slow-roll inflation should take place along an inflationary valley that can be approximated by the line $h/\phi = \sqrt{-\lambda_{H\sigma}/\lambda_H}$, where h denotes the neutral component of the Higgs doublet in the unitary gauge, while one can take $\phi = \sqrt{2}\,\mathrm{Re}\sigma$. This requires a negative portal coupling $\lambda_{H\sigma} < 0$. The potential along the valley is characterized by an effective coupling $\tilde{\lambda}_\sigma = \lambda_\sigma - \lambda_{H\sigma}^2/\lambda_H$. With the power spectrum of scalar/tensor perturbations during inflation parameterized as $\Delta^2_{s/t}(k) = A_{s/t}(k_*)\,(k/k_*)^{n_{s/t}(k_*)-1+\cdots}$, where k_* is a given reference pivot scale, the predictions for the spectral index $n_s(k_*)$ and the tensor-to-scalar ratio $r = A_t(k_*)/A_s(k_*)$ are shown in Fig. 2 for a pivot scale $k_* = 0.002\,\mathrm{Mpc}^{-1}$, together with the newest CMB constraints at the 95% confidence level arising from a combination of Planck and BICEP/KECK results [35].

In SMASH, inflation ends when $\phi \sim \mathcal{O}(M_P)$, after which the background goes through Hubble-damped oscillations that mimic a radiation fluid. Hence radiation domination starts immediately after inflation, which fixes the number of efolds $N = \Delta \log a$ –where a is the scale factor of the Friedmann-Robertson-Walker (FRW) metric– between the pivot scale's crossing of the horizon and the end of inflation. This results in the orange band in Fig. 2, providing an excellent fit to the data.

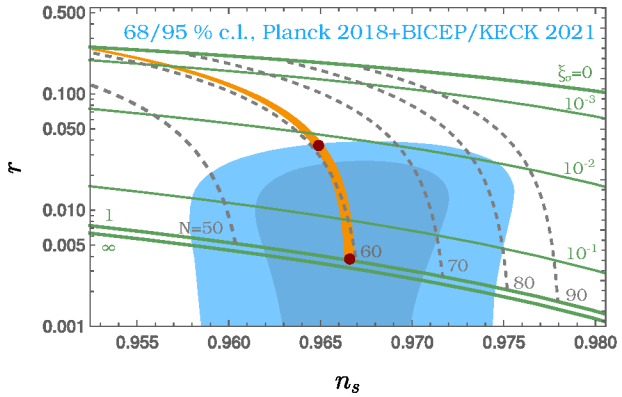

FIG. 2. Inflationary predictions in SMASH in the r vs n_s plane with a pivot scale of 0.002 Mpc^{-1}. The green solid/dashed gray lines are contours of constant ξ_σ/number of efolds, respectively. Accounting for a consistent reheating history gives the orange region, and the red dots correspond to the benchmark scenarios BP1 (upper dot) and BP2 (lower dot). We also show the 68% and 95% C.L. contours arising Planck and BICEP/KECK data [35].

For $\lambda_{H\sigma} < 0$, the oscillations of the scalar background after inflation allow for an efficient reheating. The reheating temperature was estimated in Ref. [4] to be around $T_{\mathrm{rh}} \sim 10^{10}\,\mathrm{GeV}$, under the assumption of no exponential growth of Higgs fluctuations. Such an estimate will be improved in this paper by including the Higgs field and its decays in the preheating simulations. The PQ symmetry is restored during reheating, with the axion field acquiring random values, and breaks spontaneously at later times. Around the QCD cross over, the axion field becomes massive and starts oscillating, behaving as dark matter in the so-called post-inflationary PQ symmetry breaking scenario, with the correct DM abundance reached for v_σ between $3.3 \times 10^{10}\,\mathrm{GeV}$ and $1.5 \times 10^{11}\,\mathrm{GeV}$ [36].

Benchmark points.—In order to calculate the spectrum of GWs from SMASH we fixed $f_a = 1.2 \times 10^{11}$ GeV and chose for the remaining parameters two extremal benchmark points corresponding to the maximum/minimum values of r within the allowed window $0.036 \geq r \geq 0.0037$ between the red dots of Fig. 2. We have chosen points satisfying the stability conditions of Ref. [4]. **Benchmark point 1** (BP1) has $r = 0.036$, $n_s = 0.965$, $\phi_* = 21.4 M_P$, $\phi_{\mathrm{end}} = 2.2 M_P$, $\xi_\sigma(\phi_*) = 0.014$, $\tilde{\lambda}_\sigma(\phi_*) = 1.25 \times 10^{-12}$, where field values are given in the Jordan frame, and ϕ_* is the value of

the inflaton when the CMB pivot scale crosses the horizon. The values of the Hubble scale at the crossing and at the end of inflation are $\mathcal{H}_{\rm inf}(\phi_*) = 2.0 \times 10^{-5} M_P$ and $\mathcal{H}_{\rm end} = 1.8 \times 10^{-6} M_P$. The number of post-inflationary efolds assuming radiation domination immediately after inflation is $N_{\rm post} = 64.8$. The model's couplings at the f_a scale are $\lambda_\sigma(f_a) = 3.0 \times 10^{-11}$, $\lambda_{H\sigma}(f_a) = -1.5 \times 10^{-6}$, $\lambda_H(f_a) = 0.079$, $Y_{ii}(f_a) = 1.2 \times 10^{-3}$, $y(f_a) = 8.5 \times 10^{-4}$. For **benchmark point 2** (BP2) in turn we have: $r = 0.0037$, $n_s = 0.967$, $\phi_* = 8.4 M_P$, $\phi_{\rm end} = 0.76 M_P$, $\xi_\sigma(\phi_*) = 1.0$, $\tilde{\lambda}_\sigma(\phi_*) = 5.3 \times 10^{-10}$, $\mathcal{H}_{\rm inf}(\phi_*) = 6.5 \times 10^{-6} M_P$, $\mathcal{H}_{\rm end} = 2.4 \times 10^{-6} M_P$, $N_{\rm post} = 65.0$, $\lambda_\sigma(f_a) = 4.0 \times 10^{-9}$, $\lambda_{H\sigma}(f_a) = -2.4 \times 10^{-5}$, $\lambda_H(f_a) = 0.15$, $Y_{ii}(f_a) = 4.5 \times 10^{-3}$, $y(f_a) = 3.6 \times 10^{-3}$.

Primordial GWs from SMASH.—Throughout the previously outlined cosmological history, there are three sources of stochastic GWs. First, one has GWs generated from tensor perturbations during inflation. Secondly, the exponential growth of scalar field fluctuations in the oscillating phase after inflation (preheating) generates a source term for GWs which stops when the fluctuations start to decay. Finally, after reheating is completed and the energy density is dominated by light radiation, thermal fluctuations give rise to new source-terms for GW production, which continues as long as the fermion and gauge boson abundances remain sizable, i.e. roughly until the breaking of the electroweak symmetry. In the following sections we will go over the contributions from each source to the energy fraction of GWs per logarithmic frequency interval, $\Omega_{\rm GW}(f)$, defined as $\Omega_{\rm GW} = \rho_{\rm GW0}/\rho_{c0} = \int \Omega_{\rm GW}(f) d\log f$, where $\rho_{\rm GW0}$ is the present energy density of GWs and $\rho_{c0} = 3\mathcal{H}_0^2 M_P^2$ the current total energy density. $\mathcal{H}_0 = 100\, h\, {\rm km/s/Mpc}$ is today's Hubble rate, with $h \approx 0.68$ [37].

GWs from inflation.—The spectrum of the energy fraction of primordial GWs from inflation is well known and can be approximated as [6]

$$h^2\, \Omega_{\rm iGWB}(f) \approx 9.9 \times 10^{-17} \times \\ \times\, g_{*\rho}(T_{\rm hc}(f))\, [g_{*s}(T_{\rm hc}(f))]^{-\frac{4}{3}} \left[\frac{\mathcal{H}_{\rm inf}(f)}{3 \times 10^{13}\,{\rm GeV}}\right]^2 . \quad (3)$$

Above, $\mathcal{H}_{\rm inf}(f)$ is the value of the Hubble constant when the mode corresponding to the frequency f crossed the horizon during inflation, (i.e. when $\mathcal{H} = k/a = 2\pi f a_0/a$, where a_0 is the present value of the scale factor, and k is the comoving momentum). $g_{*\rho}$ and g_{*s} denote the effective numbers of relativistic degrees of freedom associated with the energy and entropy densities, respectively – calculated for SMASH in Ref. [6] – while

$$T_{\rm hc}(f) = \frac{10^8 {\rm GeV} f}{1.2\,{\rm Hz}} \left[\frac{g_{*s}(T_{\rm hc}(f)}{g_{*\rho}(T_{\rm hc}(f))}\right]^{1/2} [g_{*s}(T_{\rm hc}(f)]^{-1/6} \quad (4)$$

is the temperature at which the mode re-entered the horizon after reheating. The spectrum of GWs during inflation for the two benchmark points in SMASH is given by the leftmost curves in Fig. 1; the vertical dashed sections represent the cutoff for frequencies that never exited the horizon during inflation [38]. When zooming into frequencies near 1 Hz, the spectra feature a step due to the PQ transition which could be detected by DECIGO [6].

GWs from preheating.—One can estimate the spectrum of GWs in terms of the time-dependent stress-energy tensor of the scalar fields by solving the linearized GW equation in momentum space in a FRW background using Green's function methods [11] (for other approaches, see for example Refs. [13, 14]). This gives [39]

$$h^2 \Omega_{\rm pGWB}(f) = h^2 \Omega_{\rm rad} \times \\ \times \left[\frac{g_{*\rho}(\tau_{\rm rh})}{g_{*\rho}(\tau_0)}\right]^{-1/3} \left[\frac{a(\tau_w)}{a(\tau_{\rm rh})}\right]^{1-3w} \left.\frac{S_k(\tau_f)}{a(\tau_w)^4 \rho(\tau_w)}\right|_{k=2\pi f a_0}, \quad (5)$$

with $S_k(\tau_f)$ given by

$$S_k(\tau_f) = \\ \frac{k^3}{2V M_P^2} \int d\Omega \sum_{m,n} \left\{ \left| \int_{\tau_i}^{\tau_f} d\tau' \cos(k\tau') a(\tau') T^{\rm TT}_{mn}(\tau', \mathbf{k}) \right|^2 \right. \\ \left. + \left| \int_{\tau_i}^{\tau_f} d\tau' \sin(k\tau') a(\tau') T^{\rm TT}_{mn}(\tau', \mathbf{k}) \right|^2 \right\}. \quad (6)$$

In the equations above, $h^2 \Omega_{\rm rad} = 4.2 \times 10^{-5}$ is the current energy fraction of radiation, τ denotes conformal time (with current value τ_0 and satisfying $d\tau/dt = 1/a$) while $\rho(\tau)$ is the total energy density. V is the 3D spatial volume, and τ_w is the moment at which the time-averaged stress-energy tensor reaches a well defined equation of state $p = w\rho$; we expect $w \approx 1/3$. $\tau_{\rm rh}$ denotes the time at which the light particles produced by the inflaton's fragmentation dominate the energy density. $T^{\rm TT}_{mn}(\tau', \mathbf{k})$ are the Fourier transforms of the spatial components of the transverse-traceless projection of the stress-energy tensor,

$$T^{\rm TT}_{mn}(\tau, \mathbf{k}) = \left(P_{mp}(\hat{\mathbf{k}}) P_{nq}(\hat{\mathbf{k}}) - \frac{1}{2} P_{mn}(\hat{\mathbf{k}}) P_{pq}(\hat{\mathbf{k}}) \right) \times \\ \times \sum_j \int \frac{d^3\mathbf{p}}{(2\pi)^{3/2}}\, p_p p_q \varphi_j(\tau, \mathbf{p}) \varphi_j(\tau, \mathbf{k} - \mathbf{p}). \quad (7)$$

In the equation above, $\hat{\mathbf{k}}$ denotes the unit vector in the direction of the 3-momentum $\mathbf{k}$, while $P_{mn}(\mathbf{k}) = \delta_{mn} - \hat{k}_m \hat{k}_n$ are transverse projectors, and the sum over j runs over all real scalar fields.

As the energy density of GWs is expected to be small, one can neglect their backreaction into the evolution of the scalar fields. To compute $h^2 \Omega_{\rm pGWB}$ from Eq. (5) we have resorted to lattice simulations of the evolution of scalar fields in a FRW background, in a similar way as described in Ref. [40]. We have solved the equations for three real scalars –the real and imaginary parts of σ

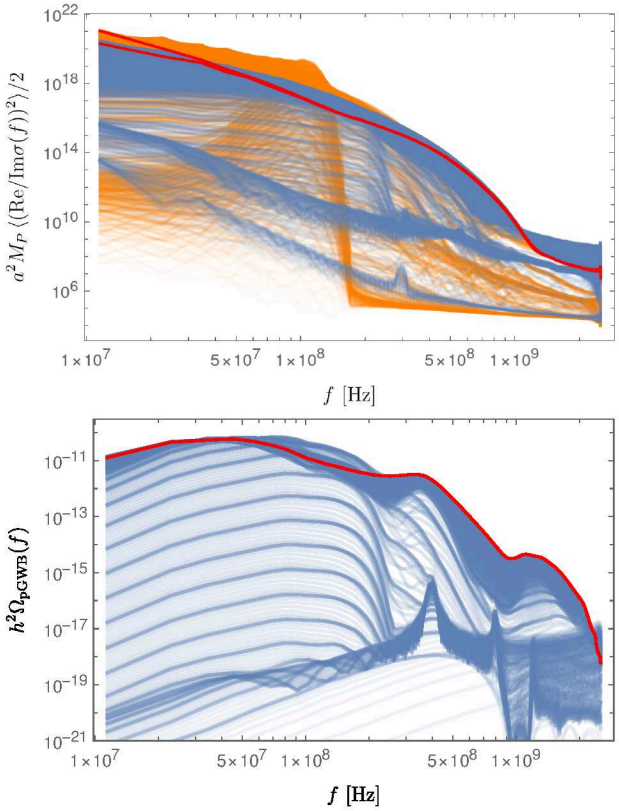

FIG. 3. Upper plot: Power spectra of $\mathrm{Re}\,\sigma$ (blue) and $\mathrm{Im}\,\sigma$ (orange) for BP1, as a function of today's frequency for subsequent values of the conformal time. Lower plot: present energy density of GWs for BP1, with the source integrated up to different times. The red lines correspond to the final time of the simulation.

and the neutral component of the Higgs– in lattices with 256^3 points. The couplings were evaluated at a renormalization scale $\mu = f_a$, and we accounted for Higgs decays by including a decay term in the Higgs' equation of motion. We modeled the decay products with a homogeneous relativistic fluid, whose density $\rho_{\rm rad}$ evolves in time ensuring the covariant conservation of the total stress-energy momentum tensor. The scale factor was also evolved in a consistent manner, and the initial conditions were determined from the backgrounds and power spectra at the end of inflation. The computations were carried out with a modified version of `CLUSTEREASY` [41, 42]; see Ref. [40] for more details. We took τ_w as the final time of the simulation and computed w using $w = -1/3(1 + 2\ddot{a}a/\dot{a}^2)$ (with $\dot{} = d/dt$). $\tau_{\rm rh}$ was inferred from the results for the energy densities, carrying out extrapolations if necessary. Assuming thermalization in the radiation bath at $\tau_{\rm rh}$, we estimated the reheating temperature as $T_{\rm rh} = (30\,\rho_{\rm rad}(\tau_{\rm rh})/(\pi^2 g_{\star\rho}(T_{\rm rh}))^{1/4}$. By matching the extrapolated Hubble rate to $\mathcal{H}_0$, accounting for the late period of matter domination, we estimated $N_{\rm post} = \log a_0/a_{\rm end}$.

The results of the simulations for BP1 are illustrated in Fig. 3, which shows the power spectra of the fields for different values of time, as well as the present energy density of GWs obtained when integrating the source up to different times. The spectra of the fields show resonance bands and peaks which are correlated (up to distortions from the convolution appearing in Eq. (7)) with the peaks in the GW spectrum. The GW spectra for both benchmark points are shown by the middle curves in Fig. 1. Dashed sections represent an extrapolation based on an f^3 behaviour for small frequencies [11], cross-checked with additional simulations.

For BP1 we infer $w = 0.3398$, $N_{\rm post} = 64.3$, $T_{\rm rh} = 9.7{\times}10^{12}$ GeV, $h^2\Omega_{\rm pGWB} = 9.5{\times}10^{-11}$, while for BP2 we obtain $w = 0.3334$, $N_{\rm post} = 65.0$, $T_{\rm rh} = 2.0\times10^{12}$ GeV, $h^2\Omega_{\rm pGWB} = 1.1\times10^{-10}$. The reheating temperatures are significantly higher than the estimates of $T_{\rm rh} \approx 10^{10}$ GeV in Ref. [4], which assumed that no resonant growth of Higgs fluctuations was possible. This is indeed the case during the first oscillations of the background after inflation, but no longer true once the fluctuations of $\mathrm{Im}\,\sigma$ start becoming amplified, lowering the Higgs mass thanks to the negative portal coupling. The resulting growth of $\rho_{\rm rad}$ is illustrated in Fig. 4.

The main features of the GW spectra can be captured by the following parameterizations,

$$f^{\rm pGWB}_{\rm peak} \simeq 3.5\times10^{13}\,{\rm Hz}\,\hat{\kappa}\sqrt{\tilde{\lambda}_\sigma}\left[\frac{\phi_{\rm end}}{M_P}\right]\left[\frac{e^{-N_{\rm post}}}{e^{-65}}\right], \quad (8)$$
$$h^2\Omega_{\rm pGWB} \simeq \frac{1.7\times10^{-7}\alpha}{\hat{\kappa}^2}\left[\frac{\mathcal{H}_{\rm end}}{5\times10^{12}\,{\rm GeV}}\right]^2\left[\frac{e^{-4N_{\rm post}}}{e^{-4\cdot65}}\right],$$

which follow from writing the typical size of field inhomogeneities during the fragmentation process as $\hat{R} = a/(\hat{\kappa}\sqrt{\tilde{\lambda}_\sigma}\phi_{\rm end}a_{\rm end})$, and estimating the energy fraction in GWs at the onset of fragmentation as $\rho_{\rm GW}(\tau_{\rm frag})/\rho(\tau_{\rm frag}) = \alpha(\hat{R}\mathcal{H}_{\rm frag})^2$ [11]. To arrive to Eq. (8) we further assumed radiation domination and $\tau_{\rm frag} \approx 200/(\sqrt{\lambda_\sigma}\phi_{\rm end}a_{\rm end})$ (see Fig. 4). Eqs. (8) can fit the peak frequency and total energy fraction in BP1/BP2 with $\hat{\kappa} = 0.05/0.08$ and $\alpha = 1\times10^{-5}/3\times10^{-4}$.

GWs from thermal fluctuations.—The Cosmic Gravitational Microwave Background (CGMB) arising from thermal fluctuations in the plasma during radiation domination has been studied in Refs. [7, 43, 44], giving

$$h^2\,\Omega_{\rm CGMB}(f) \approx 4.0\times10^{-12}\left[\frac{T_{\rm rh}}{M_P}\right]\left[\frac{g_{*s}(T_{\rm rh})}{106.75}\right]^{-5/6}\times$$
$$\times\left[\frac{f}{\rm GHz}\right]^3\hat{\eta}\left(T_{\rm rh}, 2\pi\left[\frac{g_{*s}(T_{\rm rh})}{3.9}\right]^{1/3}\frac{f}{T_0}\right), \quad (9)$$

where $T_{\rm rh}$ and T_0 denote the maximum temperature of the plasma after it starts dominating the energy density and the current CMB temperature, respectively. The function $\hat{\eta}$ is only known for low and high values of k/T. For the latter, $\hat{\eta}$ has been computed for the SM with next-to-leading order precision in Ref. [44], and the result was

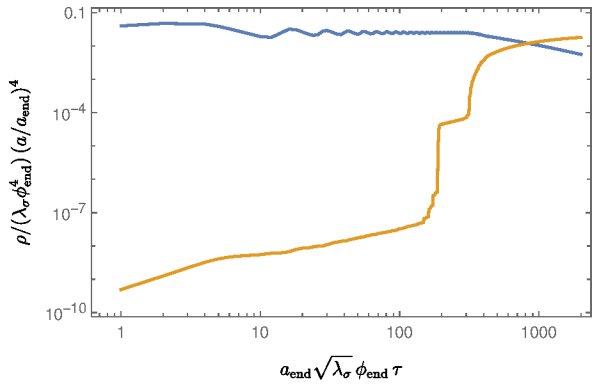

FIG. 4. Evolution of the mean energy densities of the scalars (blue) and radiation bath (orange) for BP1, giving $\tau_{\rm rh} = 835/(\sqrt{\lambda_\sigma}\phi_{\rm end}a_{\rm end})$ captured within the simulation.

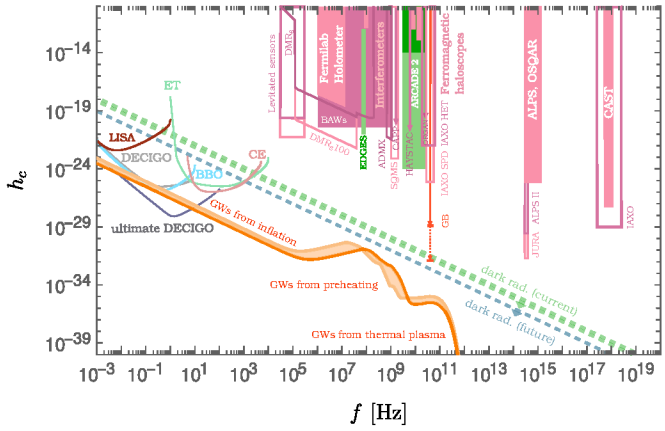

FIG. 5. Characteristic amplitude of primordial GWs in SMASH (orange) compared to present (shaded areas) and projected limits (colored solid lines) [7, 46–61]. Indirect dark radiation constraints [44, 62, 63] are shown with dashed lines.

generalized to arbitrary models in Ref. [7]. The ensuing spectrum has an amplitude scaling with $T_{\rm rh}$, and peaking at a frequency of the order of $80(106.75/(g_{*s}(T_{\rm rh}))^{1/3}$ GHz. Hence a precise measurement of the CGMB could inform us of the temperature and degrees of freedom of the primordial plasma. Using the values of $T_{\rm rh}$ inferred from the simulations, the thermal spectrum for the two benchmarks is shown by the rightmost curves in Fig. 1; the dashed lines interpolate between the results for low/high k/T.

Discussion.—The collected spectra of GWs in SMASH are shown in Fig. 1, where it can be seen that inflaton fragmentation gives the largest emission of GWs in the frequency range between $\sim 10^{5\div6}$ Hz and $10^{9\div10}$ Hz, while the inflationary GWs and the thermal GWs dominate below and above this frequency window, respectively. The peaks of the preheating and thermal spectra are well separated, and the three different components in the spectrum could be disentangled from each other if experiments were to reach the required sensitivities. A hypothetical measurement of the GW spectrum between ~ 1 Hz and 100 GHz could potentially determine the Hubble scale during inflation –which enters $\Omega_{\rm iGWB}$– the scale of inflaton fragmentation after inflation –related to $f_{\rm peak}^{\rm pGWB}$– and finally the maximum temperature and the number of relativistic degrees of freedom of the hot Big Bang plasma, which fix the amplitude and peak of $\Omega_{\rm CGMB}$. This could provide an unprecedented window into the physics of the very early universe.

We expect the main features of the spectrum of Fig. 1 to be generic and representative of a wide class of models featuring inflation and preheating followed by radiation domination. Our choice of model can be considered as a conservative benchmark, as it does not feature GWs sourced by first-order phase transitions, or an appreciable fraction of GWs from cosmic strings [45].

In Fig. 5 we show the dimensionless strain $h_c(f) = \sqrt{3\mathcal{H}_0^2\Omega_{\rm GW}(f)/(2\pi^2)}/f$ predicted in SMASH, confronted with current and projected experimental limits [7, 46–60] as well as indirect dark radiation constraints [62, 63], together with the dark radiation limit that would correspond to the theoretical uncertainty in the number of effective neutrino species [44].

In regards to the prospects for observational detection, a potential timeline could be the following. First, the upcoming generation of CMB experiments such as CMB-S4 [64], LiteBIRD [65], and the Simons Observatory [66] has the capability to detect the non-zero tensor-to-scalar ratio r predicted by SMASH (cf. Fig. 2). Given a positive measurement, future spaceborne GW interferometers such as BBO [50] or DECIGO [47] would be sensitive to $\Omega_{\rm iGWB}$ (cf. Fig. 5), while Ultimate DECIGO [67] could potentially detect the step-like feature in the spectrum at around 1 Hz due to the PQ phase transition [6]. The frequency of the step could be cross-checked with the indirect determination of f_a resulting from the potential measurement of the axion mass, $m_a \simeq 57\,\mu{\rm eV}\,(10^{11}\,{\rm GeV}/f_a)$, by axion dark matter direct detection experiments sensitive in the mass region favored in the post-inflationary PQ symmetry breaking scenario predicted by SMASH, $m_a > 28(2)\,\mu$eV [68], such as for example MADMAX [69]. Probing the waves generated by preheating and thermal effects requires much progress in the detection of ultra high frequency GWs (cf. Fig. 5). Such efforts are very well motivated by the prospect to probe physics shortly after inflation, and a worldwide initiative towards this goal has already started [70].

Acknowledgments.—We would like to thank Yvette Welling for discussions in the early stage of this project. AR acknowledges support by the Deutsche Forschungsgemeinschaft (DFG, German Research Foundation) under Germany's Excellence Strategy – EXC 2121 "Quantum Universe" – 390833306. CT acknowledges financial support by the DFG through SFB 1258 and the ORIGINS cluster of excellence.

* andreas.ringwald@desy.de
† carlos.tamarit@tum.de

[1] M. Maggiore, *Gravitational Waves. Vol. 2: Astrophysics and Cosmology* (Oxford University Press, 2018).
[2] C. Caprini and D. G. Figueroa, Class. Quant. Grav. **35**, 163001 (2018), arXiv:1801.04268 [astro-ph.CO].
[3] G. Ballesteros, J. Redondo, A. Ringwald, and C. Tamarit, Phys. Rev. Lett. **118**, 071802 (2017), arXiv:1608.05414 [hep-ph].
[4] G. Ballesteros, J. Redondo, A. Ringwald, and C. Tamarit, JCAP **08**, 001 (2017), arXiv:1610.01639 [hep-ph].
[5] G. Ballesteros, J. Redondo, A. Ringwald, and C. Tamarit, Front. Astron. Space Sci. **6**, 55 (2019), arXiv:1904.05594 [hep-ph].
[6] A. Ringwald, K. Saikawa, and C. Tamarit, JCAP **02**, 046 (2021), arXiv:2009.02050 [hep-ph].
[7] A. Ringwald, J. Schütte-Engel, and C. Tamarit, JCAP **03**, 054 (2021), arXiv:2011.04731 [hep-ph].
[8] S. Y. Khlebnikov and I. I. Tkachev, Phys. Rev. D **56**, 653 (1997), arXiv:hep-ph/9701423.
[9] R. Easther and E. A. Lim, JCAP **04**, 010 (2006), arXiv:astro-ph/0601617.
[10] R. Easther, J. T. Giblin, Jr., and E. A. Lim, Phys. Rev. Lett. **99**, 221301 (2007), arXiv:astro-ph/0612294.
[11] J. F. Dufaux, A. Bergman, G. N. Felder, L. Kofman, and J.-P. Uzan, Phys. Rev. D **76**, 123517 (2007), arXiv:0707.0875 [astro-ph].
[12] J. Garcia-Bellido and D. G. Figueroa, Phys. Rev. Lett. **98**, 061302 (2007), arXiv:astro-ph/0701014.
[13] J. Garcia-Bellido, D. G. Figueroa, and A. Sastre, Phys. Rev. D **77**, 043517 (2008), arXiv:0707.0839 [hep-ph].
[14] R. Easther, J. T. Giblin, and E. A. Lim, Phys. Rev. D **77**, 103519 (2008), arXiv:0712.2991 [astro-ph].
[15] J.-F. Dufaux, G. Felder, L. Kofman, and O. Navros, JCAP **03**, 001 (2009), arXiv:0812.2917 [astro-ph].
[16] Though there have been other efforts to estimate complete primordial spectra, such as Ref. [71], the GWs sourced by thermal fluctuations were not accounted for.
[17] R. D. Peccei and H. R. Quinn, Phys. Rev. Lett. **38**, 1440 (1977).
[18] S. Weinberg, Phys. Rev. Lett. **40**, 223 (1978).
[19] F. Wilczek, Phys. Rev. Lett. **40**, 279 (1978).
[20] J. Preskill, M. B. Wise, and F. Wilczek, Phys. Lett. B **120**, 127 (1983).
[21] L. F. Abbott and P. Sikivie, Phys. Lett. B **120**, 133 (1983).
[22] M. Dine and W. Fischler, Phys. Lett. B **120**, 137 (1983).
[23] P. Minkowski, Phys. Lett. B **67**, 421 (1977).
[24] M. Gell-Mann, P. Ramond, and R. Slansky, Conf. Proc. C **790927**, 315 (1979), arXiv:1306.4669 [hep-th].
[25] T. Yanagida, Conf. Proc. C **7902131**, 95 (1979).
[26] R. N. Mohapatra and G. Senjanovic, Phys. Rev. Lett. **44**, 912 (1980).
[27] M. Fukugita and T. Yanagida, Phys. Lett. B **174**, 45 (1986).
[28] B. L. Spokoiny, Phys. Lett. B **147**, 39 (1984).
[29] T. Futamase and K.-i. Maeda, Phys. Rev. D **39**, 399 (1989).
[30] D. S. Salopek, J. R. Bond, and J. M. Bardeen, Phys. Rev. D **40**, 1753 (1989).
[31] R. Fakir and W. G. Unruh, Phys. Rev. D **41**, 1783 (1990).
[32] F. L. Bezrukov and M. Shaposhnikov, Phys. Lett. B **659**, 703 (2008), arXiv:0710.3755 [hep-th].
[33] J. L. F. Barbon and J. R. Espinosa, Phys. Rev. D **79**, 081302 (2009), arXiv:0903.0355 [hep-ph].
[34] C. P. Burgess, H. M. Lee, and M. Trott, JHEP **09**, 103 (2009), arXiv:0902.4465 [hep-ph].
[35] P. A. R. Ade *et al.* (BICEP, Keck), Phys. Rev. Lett. **127**, 151301 (2021), arXiv:2110.00483 [astro-ph.CO].
[36] M. Buschmann, J. W. Foster, A. Hook, A. Peterson, D. E. Willcox, W. Zhang, and B. R. Safdi, Nature Commun. **13**, 1049 (2022), arXiv:2108.05368 [hep-ph].
[37] N. Aghanim *et al.* (Planck), Astron. Astrophys. **641**, A6 (2020), [Erratum: Astron.Astrophys. 652, C4 (2021)], arXiv:1807.06209 [astro-ph.CO].
[38] Assuming radiation domination after inflation, the cut-off frequency can be expressed as $f_{\rm knee}^{\Omega_{\rm iGWB}} = 7.1 \times 10^7\,{\rm Hz}\left[\frac{\mathcal{H}_{\rm end}}{5\times10^{12}\,{\rm GeV}}\right]\left[\frac{e^{-N_{\rm post}}}{e^{-65}}\right]$.
[39] We neglect here the differences between $g_{*\rho}$ and g_{*s}.
[40] G. Ballesteros, A. Ringwald, C. Tamarit, and Y. Welling, JCAP **09**, 036 (2021), arXiv:2104.13847 [hep-ph].
[41] G. N. Felder and I. Tkachev, Comput. Phys. Commun. **178**, 929 (2008), arXiv:hep-ph/0011159.
[42] G. N. Felder, Comput. Phys. Commun. **179**, 604 (2008), arXiv:0712.0813 [hep-ph].
[43] J. Ghiglieri and M. Laine, JCAP **07**, 022 (2015), arXiv:1504.02569 [hep-ph].
[44] J. Ghiglieri, G. Jackson, M. Laine, and Y. Zhu, JHEP **07**, 092 (2020), arXiv:2004.11392 [hep-ph].
[45] Although cosmic strings are formed in SMASH during the PQ phase transition, their associated energy scale fixed by $f_a \sim 10^{11}\,{\rm GeV}$ is too low to produce an appreciable GW signal.
[46] B. P. Abbott *et al.* (LIGO Scientific), Class. Quant. Grav. **34**, 044001 (2017), arXiv:1607.08697 [astro-ph.IM].
[47] N. Seto, S. Kawamura, and T. Nakamura, Phys. Rev. Lett. **87**, 221103 (2001), arXiv:astro-ph/0108011.
[48] M. Punturo *et al.*, Class. Quant. Grav. **27**, 194002 (2010).
[49] P. Amaro-Seoane *et al.* (LISA), (2017), arXiv:1702.00786 [astro-ph.IM].
[50] S. Phinney *et al.*, NASA Mission Concept Study (2004).
[51] N. Aggarwal, G. P. Winstone, M. Teo, M. Baryakhtar, S. L. Larson, V. Kalogera, and A. A. Geraci, (2020), arXiv:2010.13157 [gr-qc].
[52] A. S. Chou *et al.* (Holometer), Phys. Rev. D **95**, 063002 (2017), arXiv:1611.05560 [astro-ph.IM].
[53] M. Goryachev and M. E. Tobar, Phys. Rev. D **90**, 102005 (2014), arXiv:1410.2334 [gr-qc].
[54] T. Akutsu *et al.*, Phys. Rev. Lett. **101**, 101101 (2008), arXiv:0803.4094 [gr-qc].
[55] V. Domcke and C. Garcia-Cely, Phys. Rev. Lett. **126**, 021104 (2021), arXiv:2006.01161 [astro-ph.CO].
[56] A. Ito, T. Ikeda, K. Miuchi, and J. Soda, Eur. Phys. J. C **80**, 179 (2020), arXiv:1903.04843 [gr-qc].
[57] A. Ito and J. Soda, Eur. Phys. J. C **80**, 545 (2020), arXiv:2004.04646 [gr-qc].
[58] A. Ejlli, D. Ejlli, A. M. Cruise, G. Pisano, and H. Grote, Eur. Phys. J. C **79**, 1032 (2019), arXiv:1908.00232 [gr-qc].
[59] V. Domcke, C. Garcia-Cely, and N. L. Rodd, (2022), arXiv:2202.00695 [hep-ph].
[60] A. Berlin, D. Blas, R. Tito D'Agnolo, S. A. R. Ellis, R. Harnik, Y. Kahn, and J. Schütte-Engel, (2021),

arXiv:2112.11465 [hep-ph].
[61] K. Schmitz, 10.5281/zenodo.3689582.
[62] L. Pagano, L. Salvati, and A. Melchiorri, Phys. Lett. B **760**, 823 (2016), arXiv:1508.02393 [astro-ph.CO].
[63] T. J. Clarke, E. J. Copeland, and A. Moss, JCAP **10**, 002 (2020), arXiv:2004.11396 [astro-ph.CO].
[64] K. Abazajian *et al.*, (2019), arXiv:1907.04473 [astro-ph.IM].
[65] E. Allys *et al.* (LiteBIRD), (2022), arXiv:2202.02773 [astro-ph.IM].
[66] P. Ade *et al.* (Simons Observatory), JCAP **02**, 056 (2019), arXiv:1808.07445 [astro-ph.CO].
[67] S. Kuroyanagi, K. Nakayama, and J. Yokoyama, PTEP **2015**, 013E02 (2015), arXiv:1410.6618 [astro-ph.CO].
[68] S. Borsanyi *et al.*, Nature **539**, 69 (2016), arXiv:1606.07494 [hep-lat].
[69] P. Brun *et al.* (MADMAX), Eur. Phys. J. C **79**, 186 (2019), arXiv:1901.07401 [physics.ins-det].
[70] N. Aggarwal *et al.*, Living Rev. Rel. **24**, 4 (2021), arXiv:2011.12414 [gr-qc].
[71] W. Buchmüller, V. Domcke, K. Kamada, and K. Schmitz, JCAP **10**, 003 (2013), arXiv:1305.3392 [hep-ph].